Molecular Simulation
Vol. 35, No. 7, June 2009, 538–546

Taylor & Francis
Taylor & Francis Group

Calculation of the long-range interactions for interfacial properties

Florent Goujon, Christine Bonal and Patrice Malfreyt*

Laboratoire de Thermodynamique et Interactions Moléculaires, FRE CNRS 3099, Université Blaise Pascal, Aubière Cedex, France

(*Received 7 October 2008; final version received 1 November 2008*)

The molecular simulation of heterogeneous systems cannot be performed routinely. The results of such systems depend on the truncation procedures, size effects, long-range corrections (LRCs) to the thermodynamic properties and on the way of calculating the Coulombic interactions. We propose here to illustrate the impact of the truncation procedures on the mechanical equilibrium of the liquid–vapour interface of alkanes. The importance of the LRCs to the surface tension is established in alkanes, water, carbon dioxide and hydrogen sulphide liquid–vapour interfaces. The calculation of the electrostatic interactions in a slab geometry using a two-dimensional method and the standard three-dimensional Ewald summation technique is also reported.

Keywords: heterogeneous systems; molecular simulations; long-range corrections; Coulombic interactions

1. Introduction

Most of the phenomena in surface science (adhesion, wetting and lubrication) involve the combination of liquid–liquid, liquid–vapour and liquid–solid interfaces. Many important fundamental problems in chemistry and biology lead to practical applications in ion separation and extraction, drug delivery, oil recovery and detergents. Due to the difficulties of using experimental probes to access the molecular level structure of the interface, direct molecular simulation methods have become powerful techniques to examine the nature of the interface region and to calculate interfacial properties.

However, the molecular simulation of the heterogeneous systems cannot be considered as a routine job because the non-uniformity of the local density along the direction normal to the surface gives rise to important issues. This heterogeneity makes problems concerning the truncation procedures involved in the calculation of the force and energy equations, the long-range corrections (LRCs) to apply to the macroscopic properties and an accurate treatment of the Coulombic interactions. Additionally, when the system is modelled by a slab geometry that is periodic in two of the three directions, the calculation of the long-range Coulombic interactions cannot be applied directly.

We propose to establish the mechanical equilibrium of the liquid–vapour interface of alkanes (Figure 1(a)) in Monte Carlo (MC) and molecular dynamics (MD) simulations. This example shows the importance of the truncation procedures in the force and energy equations for the heterogeneous systems. We also show that the truncation procedures can significantly affect the results of surface tensions when they are calculated using different routes. We illustrate this point by calculating the surface tension of alkanes using both a truncated force and a force modified by a cubic spline function. We complete the study of the liquid–vapour interface by showing the order of magnitude of the LRCs to the surface tension in alkanes, water, CO_2 and H_2S systems.

In a slab geometry system, where periodic boundary conditions can be used in two of the three directions, the calculation of the long-range electrostatic interactions cannot be performed directly using the standard Ewald summation method. It requires to adapt the dimensions of the simulation box. We propose here to compare a two-dimensional method (Hautmann–Klein method, HKE) [1] and the standard three-dimensional Ewald summation (EW3D and EW3DC) techniques for the calculation of the Coulombic interactions. The two-dimensional method (HKE) [1] is better adapted to systems that are periodic in two directions only but is 20 times slower than standard three-dimensional methods. The comparison between the different methods is carried out on systems constituted of monolayers of metal-chelating ligands grafted onto a graphite surface (see Figure 1(b)). These grafted monolayers are investigated platforms in the development of applications, such as electrochemical biosensors.

2. Simulations details

2.1 Liquid–vapour interface

For the molecular simulations of the liquid–vapour interface, the total configurational energy of the systems formed

*Corresponding author. Email: patrice.malfreyt@univ-bpclermont.fr

ISSN 0892-7022 print/ISSN 1029-0435 online

DOI: 10.1080/08927020802600727
http://www.informaworld.com

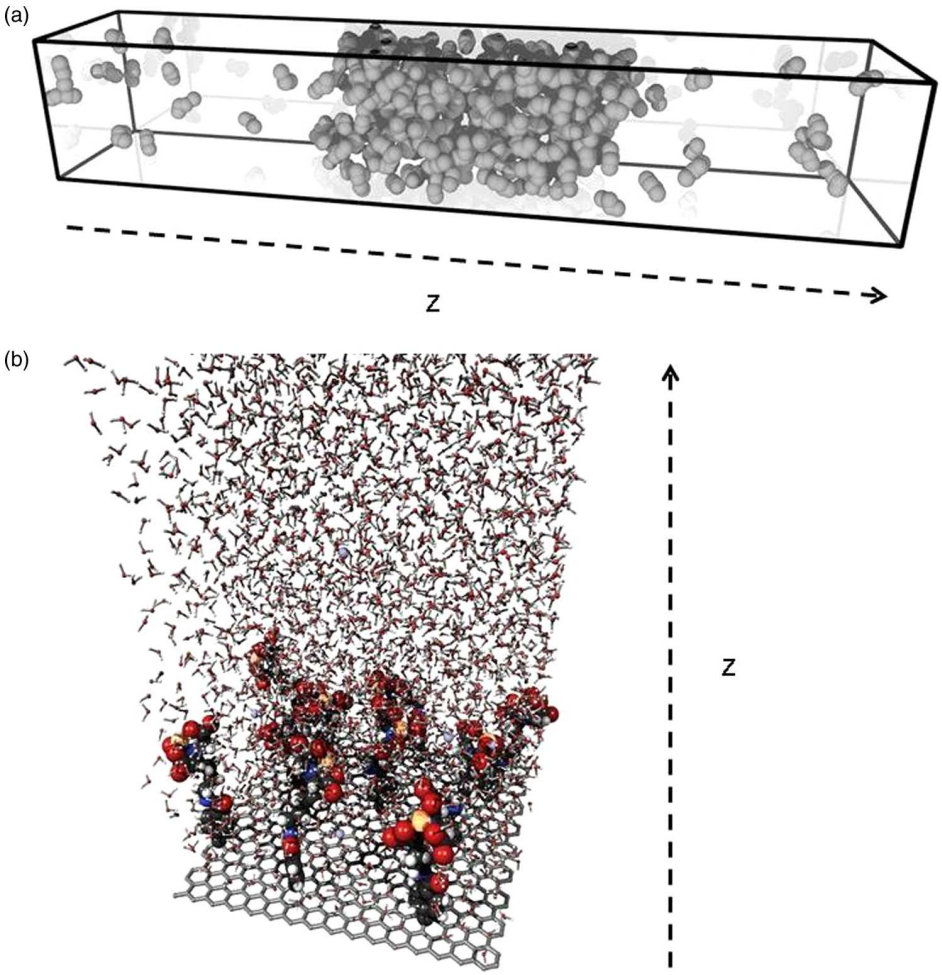

Figure 1. (a) Configurations of the *n*-pentane liquid–vapour interface at $T = 350$ K. (b) Snapshot of a MD configuration of 10 grafted NTA-Cu(II) complexed onto the HOPG surface with the water molecules.

by N molecules consists of intra- and intermolecular interactions modelled by Lennard-Jones (LJ) 6–12 sites, electrostatic point charges and a LRC contribution.

$$U = U_{\mathrm{INTRA}} + U_{\mathrm{INTER}} + U_{\mathrm{LRC}}. \tag{1}$$

The intermolecular interactions due to the repulsion–dispersion interactions are computed using the truncated LJ potential $u_{\mathrm{LJ}}(r_{iajb})$,

$$\begin{aligned} U_{\mathrm{LJ}} &= \sum_{i=1}^{N-1}\sum_{j>i}^{N}\sum_{a=1}^{N_i}\sum_{b=1}^{N_j} u_{\mathrm{LJ}}(r_{iajb}) \\ &= \sum_{i=1}^{N-1}\sum_{j>i}^{N}\sum_{a=1}^{N_i}\sum_{b=1}^{N_j} 4\varepsilon_{ab}\left[\left(\frac{\sigma_{ab}}{r_{iajb}}\right)^{12} - \left(\frac{\sigma_{ab}}{r_{iajb}}\right)^{6}\right], \end{aligned} \tag{2}$$

where r_{iajb} is the distance between the atom a in molecule i and the atom b in molecule j, ε_{ab} is the energy parameter of the interaction and σ_{ab} is the LJ core diameter. N_i is the number of atoms in the molecule i. The LJ parameters for the interactions between unlike sites are calculated using the Lorentz–Berthelot combining rules

$$\varepsilon_{ab} = (\varepsilon_{aa}\varepsilon_{bb})^{1/2} \quad \sigma_{ab} = \frac{1}{2}(\sigma_{aa} + \sigma_{bb}). \tag{3}$$

In addition to the LJ interactions, the intermolecular interactions include the total electrostatic potential U_{ELEC} calculated using the Ewald sum method [2–5] technique. For a box with orthogonal axis, U_{ELEC} is expressed as

$$\begin{aligned} U_{\mathrm{ELEC}} = {} & \frac{1}{2\varepsilon_o V}\sum_{k\neq 0} Q(h)S(\mathbf{h})S(-\mathbf{h}) \\ & + \frac{1}{8\pi\varepsilon_o}\sum_i\sum_a\sum_{j\neq i} q_{ia}\sum_b q_{jb}\,\mathrm{erfc}\,(\alpha r_{iajb}/r_{iajb}) \\ & - \frac{\alpha}{4\pi^{3/2}\varepsilon_o}\sum_i\sum_a q_{ia}^2 \\ & - \frac{1}{8\pi\varepsilon_o}\sum_i\sum_a\sum_{b\neq a}\frac{q_{ia}q_{ib}}{r_{iaib}}\,\mathrm{erf}\,(\alpha r_{iaib}), \end{aligned} \tag{4}$$

where erfc (x) is the complementary error function and erf (x) is the error function. α is chosen so that only pair interactions in the central cell need to be considered in evaluating the second term in Equation (4). The functions $S(\mathbf{h})$ and $Q(h)$ are defined using Equations (5) and (6), respectively

$$S(\mathbf{h}) = \sum_i \sum_a q_{ia} \exp(i\mathbf{h}\cdot\mathbf{r_{ia}}), \tag{5}$$

$$Q(h) = \frac{1}{h^2} \exp\left(-\frac{h^2}{4\alpha^2}\right), \tag{6}$$

where the reciprocal lattice vector $\mathbf{h}$ is defined as $\mathbf{h} = 2\pi\,(l/L_x, m/L_y, n/L_z)$, where l, m, n take values of $0, \pm1, \pm2, \ldots, \pm\infty$. The reciprocal space sum is truncated at an ellipsoidal boundary at the vector $|\mathbf{h}^{\max}|$.

As the geometry of the system shows an heterogeneity along the axis normal to the interface (z-axis), we calculate the LRC to the repulsion–dispersion energy as a function of z_k by splitting the cell into slabs of width δz. The total LRC energy U_{LRC} is then calculated by summing up all of the local contributions of each slab. The LRCs to the total energy within each kth slab are defined by two parts [6],

$$U_{\mathrm{LRC}} = \sum_{i=1}^{N_s} u_{\mathrm{lrc}}(z_k) = \sum_{i=1}^{N_s} \left(u_{\mathrm{lrc}}^{(1)}(z_k) + u_{\mathrm{lrc}}^{(2)}(z_k)\right) \quad \text{with}$$

$$u_{\mathrm{lrc}}^{(1)}(z_k) = \frac{8\pi}{3}\rho(z_k)^2 V_s \sum_{a=1}^{N_i}\sum_{b=1}^{N_j} \varepsilon_{ab}\left[1/3\left(\frac{\sigma_{ab}^{12}}{r_c^9}\right) - \left(\frac{\sigma_{ab}^{6}}{r_c^3}\right)\right] \tag{7}$$

$$u_{\mathrm{lrc}}^{(2)}(z_k) = \pi\rho(z_k)V_s \int_{r_c}^{\infty} \mathrm{d}r \times \int_{-r}^{r} \mathrm{d}\Delta z \sum_{i=1}^{N_s} \left[\rho(z_{k+i}) - \rho(z_{k+i-1})\right] r U_{\mathrm{LJ,m}}(r), \tag{8}$$

where $\rho(z_k)$ and V_s are, respectively, the density and the volume of the slab k. Δz is defined as the difference $z - z_k$. N_s is the number of slabs between z and z_k. r_c is the cut-off radius, $U_{\mathrm{LJ,m}}(r)$ is the intermolecular energy and r is the distance between the two centres of mass.

$$U_{\mathrm{LJ,m}}(r) = \sum_a^{N_i}\sum_b^{N_j} 4\varepsilon_{ab}\left[\left(\frac{\sigma_{ab}}{r}\right)^{12} - \left(\frac{\sigma_{ab}}{r}\right)^{6}\right]. \tag{9}$$

The first part of the long-range contribution has an analytical form identical to the one associated with a homogeneous system but uses the local density $\rho(z_k)$ of the slab. The second part consists of a double integral that contains a series of density differences, which render this part cumbersome to calculate.

2.2 Grafted metal-chelating monolayers onto a graphite surface

For the modelling of the grafted monolayers, we used the all-atom (AA) version of the Cornell force field AMBER [7]. The general potential function is of the form

$$\begin{aligned} U = {} & \sum_{\text{bonds}} k_b(r - r_o)^2 + \sum_{\text{angles}} k_\theta(\theta - \theta_o)^2 \\ & + \sum_{\text{dihedrals}} k_\phi[1 + \cos(l\phi + \delta)] \\ & + \sum_{i=1}^{N-1}\sum_{j=i+1}^{N} \left\{ 4\varepsilon_{ij}\left[\left(\frac{\sigma_{ij}}{r_{ij}}\right)^{12} - \left(\frac{\sigma_{ij}}{r_{ij}}\right)^{6}\right] \right. \\ & \left. + \sum_{l}^{\infty\prime} \frac{q_i q_j}{|\mathbf{r_{ij}} + \mathbf{n}L|} \right\}, \end{aligned} \tag{10}$$

where k_b, k_θ and k_ϕ are the force constants for deformation of bonds, angles and dihedrals, respectively. The equilibrium values of bond distances and valence angles correspond to r_o and θ_o, respectively. In the dihedral angle term, l is the periodicity and δ is the phase factor. The intermolecular and intramolecular interactions consist of a van der Waals repulsion–dispersion term calculated using the LJ (6–12) potential, represented by the penultimate term in Equation (10). In the AMBER force field, the non-bonded interactions between atoms separated by exactly three bonds (1–4 van der Waals interactions) are reduced by a factor of 0.5 [7]. The LJ potential parameters for the interactions between unlike atoms were calculated by using the Lorentz–Berthelot mixing rules (quadratic and arithmetic rules for ε_{ij} and σ_{ij} parameters, respectively). The water molecules were represented with the TIP4P/2005 model [8].

When the last term in Equation (10) is calculated with Equation (4), the method is called EW3D and refers to the standard Ewald summation technique. When Equation (4) is changed by the addition of $(1/2\varepsilon_o V)M_z^2$, the method is called EW3DC. M_z is the net dipole moment of the simulation cell given by $\sum_{i=1}^{N} q_i \mathbf{r}_i$. This contribution is the correction term from Yeh and Berkowitz [9], which results by the plane-wise summation method proposed by Smith [3]. Adding this term to the total energy amounts to using a z-component force for each atom given by

$$F_{i,z} = -\frac{q_i}{\varepsilon_o V} M_z. \tag{11}$$

The EW3DC method differs from the standard EW3D method only by the presence of this dipole correction. However, these two three-dimensional method require to change the primary simulation box by adding two empty spaces between the periodic image in order to dampen out the interslab interactions [9–11].

The total Coulombic interactions for a two-dimensional periodic system, which is finite in the z-dimension, can be

calculated using the Hautman and Klein method [1]. This method is in fact an adaptation of the Ewald technique for systems that are periodic in two dimensions only. The operational expressions of the total electrostatic interactions can be found elsewhere [1] for completeness.

The computational procedures of the molecular simulation of the liquid–vapour interface can be found in previous papers [12–17]. The force field used in the molecular modelling of the grafted system and the description of the computational procedures can also be found elsewhere [11]. Figure 1(a),(b) shows typical configurations of the liquid–vapour interface of the *n*-pentane and of the NTA grafted system, respectively. In these snapshots, z refers to the direction of the heterogeneity.

3. Results and discussions

We propose here to illustrate the importance of the truncation procedures for the mechanical equilibrium of the liquid–vapour interface of alkanes. The impact of the discontinuities in the force and energy equations is also studied for the different definitions of the surface tension. The LRCs to the surface tension are reported for systems involving both electrostatic and dispersion–repulsion energy contributions. We finish by the calculation of the electrostatic interactions in a slab geometry system.

3.1 Calculation of the normal and tangential pressure components

In the case of a planar liquid–vapour surface lying in the x,y plane, where the heterogeneity takes place along the z direction normal to the surface, the calculation of the normal and tangential pressure components along this axis is meaningful for the validation of the mechanical equilibrium. The components of the pressure tensor calculated from the Irving and Kirkwood definition [18–20] are expressed by

$$p_{\alpha\beta}(z_k) = \langle \rho(z_k) \rangle k_B T \mathbf{I} + \frac{1}{A} \left\langle \sum_{i=1}^{N-1} \sum_{j>i}^{N} (\mathbf{r}_{ij})_\alpha (\mathbf{F}_{ij})_\beta \times \frac{1}{|z_{ij}|} \theta\left(\frac{z_k - z_i}{z_{ij}}\right) \theta\left(\frac{z_j - z_k}{z_{ij}}\right) \right\rangle, \quad (12)$$

where $\mathbf{I}$ is the unit tensor and T is the input temperature. α and β represent x, y or z directions. $\theta(x)$ is the unit step function defined by $\theta(x) = 0$ when $x < 0$, and $\theta(x) = 1$ when $x \geq 0$. A is the surface area normal to the z-axis. The distance z_{ij} between two molecular centres-of-mass is divided into N_s slabs of thickness δz. Following Irving and Kirkwood, the molecules i and j give a local contribution to the pressure tensor in a given slab if the line joining the centres-of-mass of molecules i and j crosses, starts or finishes in the slab. Each slab has $1/N_s$ of the total contribution from the $i-j$ interaction. The normal component $p_N(z_k)$ is equal to $p_{zz}(z_k)$, whereas the tangential component is given by $(1/2)(p_{xx}(z_k) + p_{yy}(z_k))$. $\mathbf{F}_{ij}$ in Equation (12) is the intermolecular force between the molecules i and j, and is expressed as the sum of all the site–site forces acting between these two molecules.

$$\mathbf{F}_{ij} = \sum_{a=1}^{N_i} \sum_{b=1}^{N_j} (\mathbf{f}_{iajb}) = -\sum_{a=1}^{N_i} \sum_{b=1}^{N_j} \frac{\mathbf{r}_{iajb}}{r_{iajb}} \frac{\mathrm{d}U(r_{iajb})}{\mathrm{d}r_{iajb}}. \quad (13)$$

For the simulation of the liquid–vapour interface of alkanes, the total intermolecular energy U is calculated by using the LJ potential U_{LJ} because no electrostatic interactions are involved in the model. In our MC simulations, the LJ potential is truncated at the cut-off radius ($r_c = 12$ Å) according to U_T

$$U_T(r_{iajb}) = \begin{cases} U_{LJ}(r_{ij}) & r_{iajb} < r_c; \\ 0 & r_{iajb} \geq r_c. \end{cases} \quad (14)$$

The calculation of the pressure components requires the use of the derivative of the potential. This derivative can be calculated using either the truncated force expressed as

$$f_T(r_{iajb}) = \begin{cases} -\frac{\partial U_{LJ}}{\partial r_{iajb}} & r_{iajb} < r_c; \\ 0 & r_{iajb} \geq r_c, \end{cases} \quad (15)$$

or the truncated force modified by the addition of an impulse contribution [21] defined by

$$f_{TC}(r_{iajb}) = \begin{cases} -\frac{\partial U_{LJ}}{\partial r_{iajb}} & r_{iajb} < r_c; \\ +\frac{U_{LJ}(r_c)}{\Delta r} & r_c < r_{iajb} < r_c + \Delta r; \\ 0 & r_{iajb} \geq r_c + \Delta r, \end{cases} \quad (16)$$

where Δr is equal to 0.05 Å for a cut-off of 12 Å. In most of the cases, the MD simulations used a truncated force and the MC simulations a truncated potential. Figure 2 shows the profiles of the normal p_N and tangential p_T components of the pressure tensor calculated from the MC and MD configurations. For a planar surface, the mechanical equilibrium requires to have $p_N(z)$ and $p_T(z)$ constant and equal to p in the bulk phases. In the interfacial region, p_T exhibits two negative peaks indicating that the liquid phase is under tension. The normal and tangential components of the pressure calculated from MD are shown in Figure 2(a). These profiles establish the mechanical equilibrium of these MD configurations as expected for

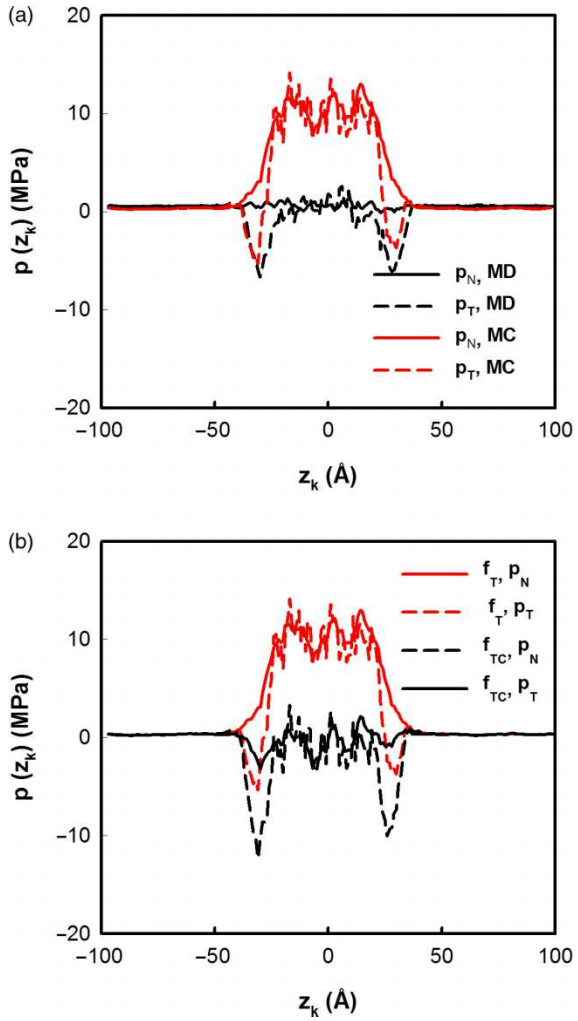

Figure 2. Normal and tangential pressure components calculated in the liquid–vapour interface of the *n*-pentane at $T = 325$ K from (a) MC using a truncated potential and MD using a truncated force and (b) MC using both a truncated force f_T and a truncated force modified by an additional impulse f_{TC}.

a method that uses the forces to generate the evolution of the system. On the other hand, in MC configurations when the forces are calculated from Equation (15), the profiles of p_N and p_T highlight that the configurations are not in the mechanical equilibrium. This can be explained by the fact that MC uses the configurational energy to generate the configurations and that the pressure is calculated from the derivative of the configurational energy. When the configurational energy is calculated with a truncated potential that is not differentiable at the cut-off radius, the truncated force used in the calculation of the pressure does not correspond to the truncated potential. To match the force and energy equations, the force must be corrected by an addition term. When the force is corrected as in Equation (16), the profiles of the normal and tangential components of Figure 2(b) show that the mechanical equilibrium is satisfied within the MC configurations.

Another way of removing the discontinuities in the energy and force equations is to use the LJ potential modified by a cubic spline. The potential and force equations become

$$U_{SP}(r_{iajb}) = \begin{cases} U_{LJ}(r_{iajb}) - U_{LJ}(r_s) + a & r_{iajb} < r_s; \\ -\frac{b}{3}(r_{iajb} - r_c)^3 - \frac{c}{4}(r_{iajb} - r_c)^4 & r_s \le r_{iajb} < r_c; \\ 0 & r_{iajb} \ge r_c, \end{cases} \tag{17}$$

$$f_{SP}(r_{ij}) = \begin{cases} -\dfrac{\partial U_{LJ}}{\partial r_{iajb}} & r_{iajb} < r_s; \\ +b(r_{iajb} - r_c)^2 + c(r_{iajb} - r_c)^3 & r_s \le r_{iajb} < r_c; \\ 0 & r_{iajb} \ge r_c. \end{cases} \tag{18}$$

Using such expressions, the potential and its derivative are continuous at the cut-off. The parameters a, b and c are calculated by requiring that the first and second derivatives of the u_{SP} potential be continuous at r_s and r_c.

$$\begin{aligned} c &= +\frac{\partial^2 U_{LJ}}{\partial r_{ij}^2}(r_s)/(r_s - r_c)^2 - 2\frac{\partial U_{LJ}}{\partial r_{ij}}(r_c)/(r_s - r_c)^3 \\ b &= -\frac{\partial^2 U_{LJ}}{\partial r_{ij}^2}(r_s)/(r_s - r_c) + 3\frac{\partial U_{LJ}}{\partial r_{ij}}(r_s)/(r_s - r_c)^2 \\ a &= -\frac{b}{3}(r_s - r_c)^3 - \frac{c}{4}(r_s - _c)^4. \end{aligned} \tag{19}$$

Figure 3(a),(b) displays the profiles of the normal and tangential pressure components calculated over the MC and MD configurations using the potential and force of Equations (17) and (18), respectively. The profiles match very well within the MC and MD methods and indicate the primary importance of the discontinuity of the potential at the cut-off. Additionally, the total local chemical potential calculated from Equation (20) exhibits a flat profile as expected for a planar liquid–vapour interface at the equilibrium:

$$\mu(z_k) = kT \ln\left(\left\langle \frac{\Lambda^3 \rho(z_k)}{\exp(-\Delta U/k_B T)} \right\rangle_{z_k,NVT}\right), \tag{20}$$

where Λ is the de Broglie thermal wavelength and U is the potential changed by a cubic spline function. ΔU represents the energy of the ghost $(N+1)$ particle with the N particles. The local expression of the chemical potential was established by Widom [22].

The discontinuity in the force and energy equations was not considered as crucial in the simulations

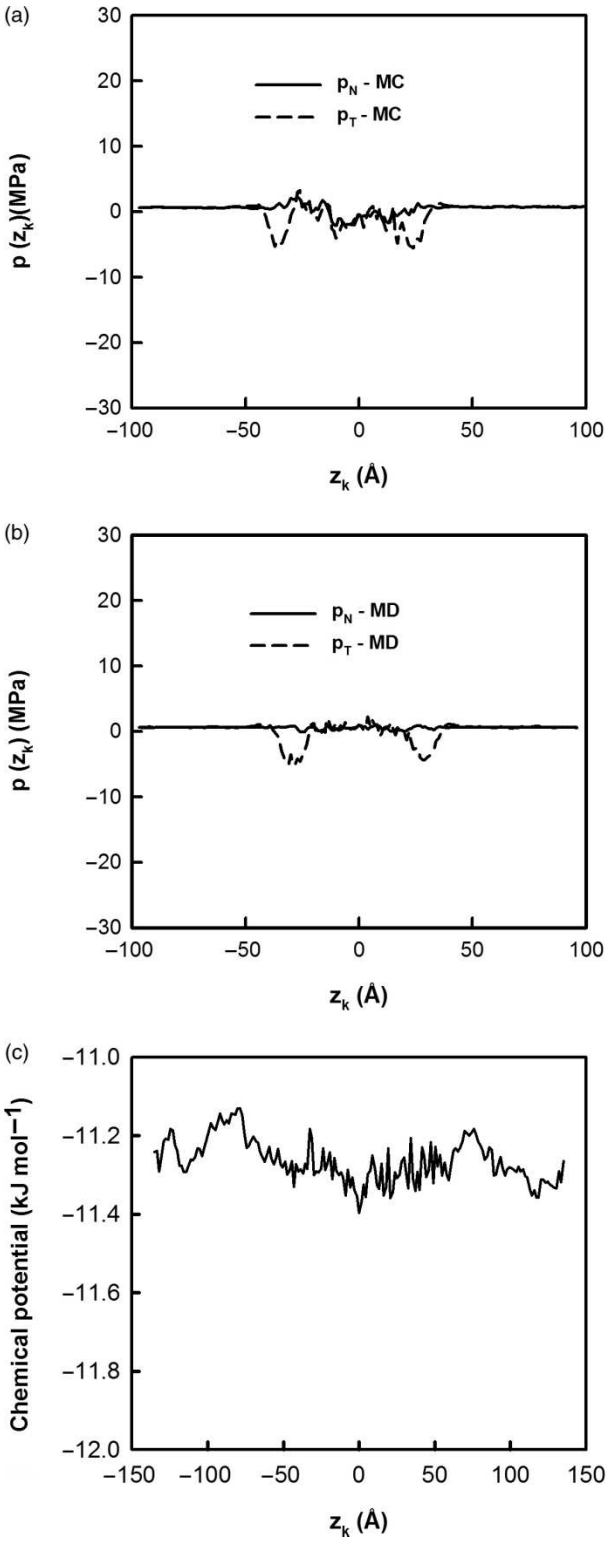

Figure 3. Normal and tangential pressure components calculated in the liquid–vapour interface of the *n*-pentane at $T = 325$ K from (a) MC and (b) MD using a LJ potential and a force changed by a cubic spline function. (c) Total chemical potential of the liquid–vapour interface of methane at $T = 120$ K calculated from MC simulations using a LJ potential changed by a cubic spline function.

of a homogeneous fluid, where there was a compensation between the forces affecting a particle from outside its cut-off sphere. In the case of heterogeneous system, this assumption is no longer valid and the equivalence between MC and MD is recovered only when the discontinuities are removed. In this case, the MC and MD simulations are performed with the same potential.

3.2 Calculation of the surface tension

In the case of the calculation of the surface tension, the discontinuities in the energy and force expressions can lead to significant differences between the different routes. Some definitions use the potential energy in their working expressions. For instance, the test-area (TA) method [23] recently developed uses the perturbation formalism to express the surface tension. Other expressions (KB [24] and IK [19,20,25]) are based upon the mechanical definition of the surface tension and use the derivative of the potential in their operational expressions. Table 1 shows that the intrinsic part of the surface tension calculated from the potential energy (TA) is different from that calculated from the derivative of the potential energy (IK,KB). However, when the discontinuities are removed in the expressions of the force and energy with a cubic spline function, the intrinsic part is identical within IK, KB and TA approaches. The equivalence between the different operational expressions can also be recovered by making the potential and force equations consistent [14].

Another important contribution to the surface tension is the long-range contribution due to the fact that interactions are neglected from the cut-off region. The appropriate LRC of the normal and tangential components of the pressure tensor within the IK definition have been derived by Guo and Lu [6] and are composed of two parts as expressed in Equations (21) and (22).

$$\begin{aligned} p_{\mathrm{N,LRC}}(z_k) &= p^{(1)}_{\mathrm{N,LRC}}(z_k) + p^{(2)}_{\mathrm{N,LRC}}(z_k) \\ &= -\frac{2\pi}{3}\rho^2(z_k)\int_{r_c}^{\infty} \mathrm{d}r r^3 \frac{\mathrm{d}U_{\mathrm{LJ,m}}(r)}{\mathrm{d}r} \\ &\quad - \pi\rho(z_k)\int_{r_c}^{\infty}\mathrm{d}r\int_{-r}^{r}\mathrm{d}\Delta z\,[\rho(z)-\rho(z_k)]\frac{\mathrm{d}U_{\mathrm{LJ,m}}(r)}{\mathrm{d}r}(\Delta z)^2. \end{aligned} \tag{21}$$

Table 1. Surface tensions of methane (mN m^{-1}) calculated from MC simulations using a truncated LJ potential and a modified LJ potential using the KB, IK and TA approaches.

	γ_{KB}	γ_{IK}	γ_{TA}
Truncated potential	9.5	9.5	10.6
Spline potential	8.5	8.5	8.5

The cut-off radius is fixed to 12 Å.

As concerns the tangential pressure, the first term is identical to the first term of the normal component whereas the second term is expressed by

$$p^{(2)}_{\mathrm{T,LRC}}(z_k) = -\frac{\pi}{2}\rho(z_k)\int_{r_c}^{\infty}\mathrm{d}r\int_{-r}^{r}\mathrm{d}\Delta z\,[\rho(z)-\rho(z_k)] \times \frac{\mathrm{d}U_{\mathrm{LJ,m}}(r)}{\mathrm{d}r}\left[r^2-(\Delta z)^2\right]. \quad (22)$$

The first term of $p_{\mathrm{N,LRC}}(z_k)$ and $p_{\mathrm{T,LRC}}(z_k)$ is identical to that used in homogeneous molecular simulations by using a local density $\rho(z_k)$ instead of a scalar density ρ, whereas the second term takes into account the density differences between the slabs. From these LRC expressions, it is then possible to calculate the LRC parts relative to the surface tension. From a mechanical viewpoint, the surface tension can also be calculated from the integration of the difference of the normal and tangential components of the pressure tensor [18–20] across both interfaces according to

$$\gamma = \gamma_{\mathrm{I}} + \gamma_{\mathrm{LRC}} \quad (23)$$

$$= \frac{1}{2}\int_{-L_z/2}^{+L_z/2}\mathrm{d}z\big(p_{\mathrm{N}}(z_k)-p_{\mathrm{T}}(z_k)\big) + \frac{1}{2}\int_{-L_z/2}^{+L_z/2}\mathrm{d}z\big(p_{\mathrm{N,LRC}}(z_k)-p_{\mathrm{T,LRC}}(z_k)\big), \quad (24)$$

where the first term is related to the intrinsic part of the surface tension and the second one corresponds to the LRC part.

Figure 4(a) shows the profiles of the difference between the normal and tangential components as a function of the z-direction. We observe that the two profiles are well symmetric with a well-established liquid bulk phase. The integral of the profile is represented on the right axis. The integral allows to check that the contributions to the surface tension are the same for the two interfaces with a flat profile between them. Figure 4(b) plots the profile of the LRCs to $p_{\mathrm{N}} - p_{\mathrm{T}}$ difference with the integral of this property represented on the right axis. The profile of the LRCs to the pressure components indicates that the contribution of each interface is identical and there is no contribution in the bulk phases. The total value of the LRC to the surface tension is far from being negligible: in this case, it represents up to 30% of the total surface tension. The calculation of the surface tension requires the use of appropriate LRCs; each operational expression of the surface tension must be corrected by specific LRCs. This was described in detail elsewhere [14]. Interestingly, Table 2 shows the intrinsic surface tension with its LRCs for some alkanes, water, carbon dioxide and hydrogen sulphide. In water, the LRCs to the surface tension are small whereas the electrostatic contribution to the surface tension is negative. In CO_2 and H_2S, the dispersion–repulsion contributions are greater than the electrostatic interactions; the LRCs to the surface tension then represent about 30% of the total value.

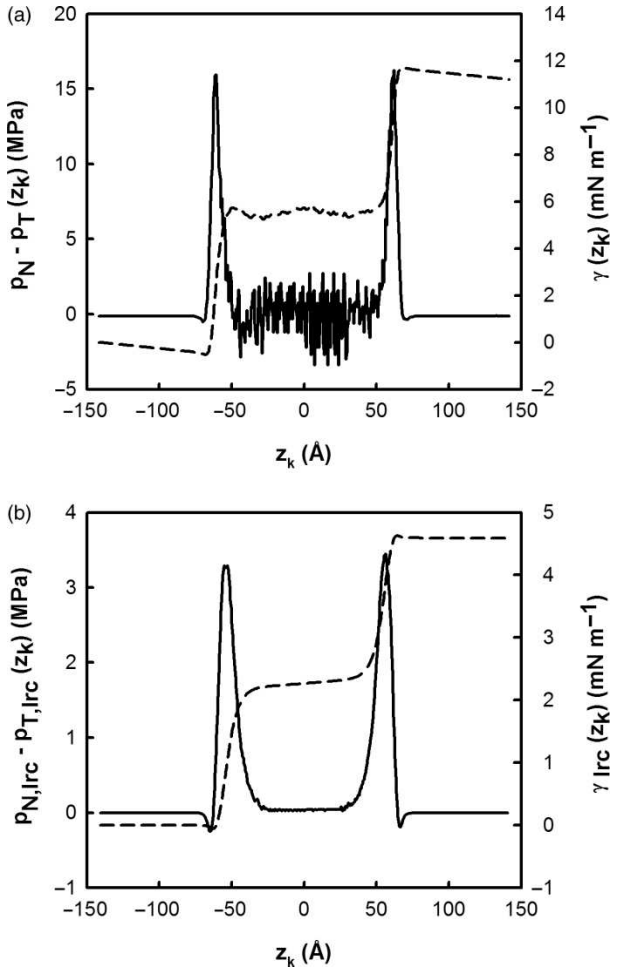

Figure 4. (a) Difference between the normal and tangential pressure profiles for the liquid–vapour interface of the *n*-pentane at $T = 300$ K; (b) difference between the normal and tangential components of the LRCs to the pressure tensor. On the right axis, the integral of each difference is plotted as a function of z.

Table 2. Lennard-Jones, electrostatic and long range corrections contributions to the surface tension (mN m^{-1}) calculated from MC simulations in different liquid–vapour systems.

	γ_{LJ}	γ_{ELE}	γ_{LRC}	γ_{TOT}	γ_{EXP}
CH_4	9.5		3.8	13.3	11.3
nC_5	12.0		5.6	17.6	15.3
nC_{10}	6.0		4.3	10.3	10.4
H_2O	−87.6	117.7	3.5	33.6	36.5
CO_2	6.1	2.9	2.5	11.5	12.0
H_2S	21.0	9.3	8.0	38.3	37.5

3.3 Calculation of the electrostatic interactions in a slab geometry

The calculation of the electrostatic interactions in a system represented by a slab geometry must be carefully undertaken. The use of a two-dimensional method such

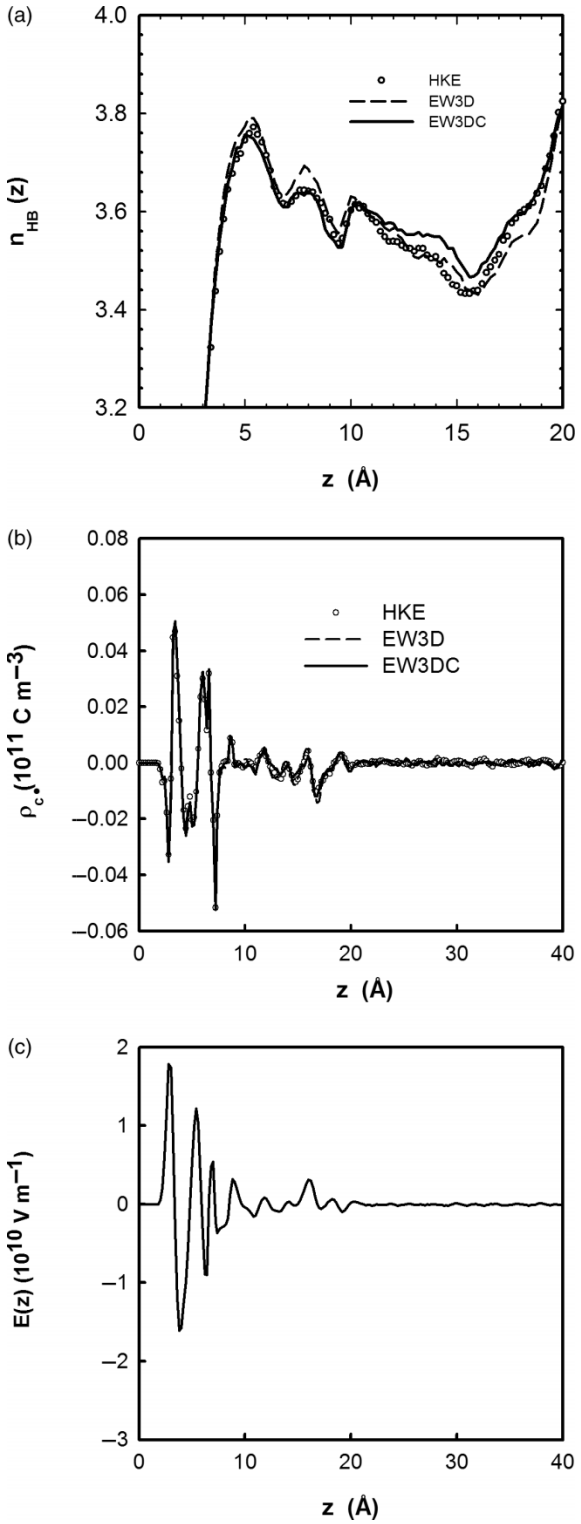

Figure 5. (a) Profiles of the number of hydrogen bonds between water molecules along the direction normal to the surfaces. (b) Charge density and (c) electric field profiles along the direction normal to the surface.

as the Hautmann–Klein method (HKE) [1] is recommended for systems that are periodic in two dimensions only. However, the two-dimensional methods are cumbersome and time consuming. The HKE method is about 20 times slower than the standard Ewald methods (EW3D and EW3DC). It is then fundamental from a methodological viewpoint to check that the two- and three-dimensional methods lead to the same energetic, structural and electrical properties in slab geometry systems. We propose to check these points on a system formed by negatively charged monolayers of chelating copper (NTA) compounds immobilised onto a HOPG graphite surface in aqueous solution. The use of a three-dimensional method in a slab geometry system requires to elongate the simulation box in the z-direction in order to dampen out the interslab interactions. Figure 5(a) depicts the number of hydrogen bonds between water molecules in the region close to the surface. The criteria used for the calculation of the number of hydrogen bonds can be found in a previous paper [11]. This figure demonstrates that the number of hydrogen bonds between water molecules close to the grafted surface does not depend on the method used for the calculation of the electrostatic interactions indicating that KHE, EW3D and EW3DC methods give the same structure of water. The charge density profiles of water molecules are reported in Figure 5(b) for each method. This figure tends to establish that the distribution of charges of water molecules is slightly perturbed close to the surface. This is due to the presence of grafted molecules that are able to interact preferentially with water molecules to give hydrogen bonds. However, from 20 Å, the charge density profile recovers an expected zero value. We observe that the three methods give the same charge density profiles. The analysis of the electric field profile $E(z)$ (Figure 5(c)) calculated from the integral of the charge density profile confirms that the electric field reaches a constant zero from 20 Å. From this value of z, the distribution of water molecules is isotropic as expected for a bulk-like region. This indicates that the surface and the grafted molecules do not significantly influence the water molecules within this region. Additionally, the calculation of these electric properties allows to validate the use of three-dimensional methods for the calculation of the Coulombic interactions in a slab geometry.

4. Conclusions

We have shown that the use of truncated potential and truncated force may lead to significant differences in the mechanical equilibrium and surface tensions of liquid–vapour systems governed by dispersion–repulsion interactions. Removing the discontinuities in the potential and

force equations amount to recovering the equivalence between MC and MD and to making consistent the different routes of the calculation of the surface tension. Whereas the effects of these discontinuities are compensated in the simulation of bulk phases, they must be taken into account in the simulation of the two-phase systems.

The simulation of slab geometry system requires to do a compromise between an accurate treatment of the Coulombic interactions, the use of fully developed system and the number of steps to obtain a good convergence of the thermodynamic and electrical properties. A solution consists in using a slightly modified EW3D method with the addition of empty space between the primary simulation cells. We have compared the results between the three-dimensional methods and a two-dimensional method. We have concluded that the standard Ewald summation technique can be used with confidence in such slab geometries.

References

[1] J. Hautmann and M.L. Klein, *An Ewald summation method for planar surfaces and interfaces*, Mol. Phys. 75 (1992), pp. 379–395.

[2] M.P. Allen and D.J. Tildesley, *Computer Simulation of Liquids*, Clarendon Press, Oxford, 1989.

[3] E.R. Smith, *Electrostatic energy in ionic crystals*, Proc. R. Soc. Lond. A 375 (1981), pp. 475–505.

[4] D.M. Heyes, *Pressure tensor of partial-charge and point-dipole lattices with bulk and surface geometries*, Phys. Rev. B 49 (1994), pp. 755–764.

[5] J. Alejandre, D.J. Tildesley, and G.A. Chapela, *Molecular dynamics simulation of the orthobaric densities and surface tension of water*, J. Chem. Phys. 102 (1995), pp. 4574–4583.

[6] M. Guo and B.C.Y. Lu, *Long range corrections to thermodynamic properties of inhomogeneous systems with planar interfaces*, J. Chem. Phys. 106 (1997), pp. 3688–3695.

[7] W.D. Cornell, P. Cieplak, C.I. Bayly, I.R. Gould, K.M. Merz, D.M. Ferguson Jr, D.M. Fox, T. Spellemer, J.W. Caldwell, and P. Kolleman, *A second generation force field for the simulation of proteins, nucleic acids, and organic molecules*, J. Am. Chem. Soc. 117 (1995), pp. 5179–5197.

[8] J.L.F. Abascal and C. Vega, *A general purpose model for the condensed phases of water: Tip4p/2005*, J. Chem. Phys. 123 (2005), 234505.

[9] I.C. Yeh and M.L. Berkowitz, *Ewald summation for systems with slab geometry*, J. Chem. Phys. 111 (1999), pp. 3155–3162.

[10] S. Crozier, R.L. Rowley, E. Spohr, and D. Henderson, *Comparison of charged sheets and corrected 3d Ewald calculations of long-range forces in slab geometry electrolyte systems with solvent molecules*, J. Chem. Phys. 112 (2000), pp. 9253–9257.

[11] F. Goujon, C. Bonal, B. Limoges, and P. Malfreyt, *Molecular simulations of grafted metal-chelating monolayers: methodology, structure and energy*, Mol. Phys. 106 (2008), pp. 1397–1411.

[12] F. Goujon, P. Malfreyt, A. Boutin, and A.H. Fuchs, *Direct Monte Carlo simulations of the equilibrium properties of the n-pentane liquid–vapor interface*, J. Chem. Phys. 116 (2002), pp. 8106–8117.

[13] F. Goujon, P. Malfreyt, J.M. Simon, A. Boutin, B. Rousseau, and A.H. Fuchs, *Monte Carlo versus molecular dynamics simulations in heterogeneous systems: an application to the n-pentane liquid–vapor interface*, J. Chem. Phys. 121 (2004), pp. 12559–12571.

[14] C. Ibergay, A. Ghoufi, F. Goujon, P. Ungerer, A. Boutin, B. Rousseau, and P. Malfreyt, *Molecular simulations of the* n*-alkane liquid–vapour interface: interfacial properties and their long range corrections*, Phys. Rev. E 75 (2007), 051602.

[15] A. Ghoufi, F. Goujon, V. Lachet, and P. Malfreyt, *Expressions for local contributions to the surface tension from the viral route*, Phys. Rev. E 77 (2008), 031601.

[16] A. Ghoufi, F. Goujon, V. Lachet, and P. Malfreyt, *Calculation of the surface tension of acid gazes and water from Monte Carlo simulations*, J. Chem. Phys. 128 (2008), 154716.

[17] A. Ghoufi, F. Goujon, V. Lachet, and P. Malfreyt, *Multiple histogram reweighting method for the surface tension calculation*, J. Chem. Phys. 128 (2008), 154718.

[18] J.S. Rowlinson and B. Widom, *Molecular Theory of Capillarity*, Clarendon Press, Oxford, 1982.

[19] J.P.R.B. Walton, D.J. Tildesley, J.S. Rowlinson, and J.R. Henderson, *The pressure tensor at the planar surface of a liquid*, Mol. Phys. 48 (1983), pp. 1357–1368.

[20] J.P.R.B. Walton and K.E. Gubbins, *The pressure tensor in an inhomogeneous fluid of non-spherical molecules*, Mol. Phys. 58 (1986), p. 1013.

[21] A. Trokhymchuk and J. Alejandre, *Computer simulations of liquid/vapor interface in Lennard-Jones fluids: some questions and answers*, J. Chem. Phys. 111 (1999), pp. 8510–8523.

[22] B. Widom, *Structure of interfaces from uniformity of the chemical potential*, J. Stat. Phys. 19 (1978), pp. 563–574.

[23] G.J. Gloor, G. Jackson, F.J. Blas, and E. de Miguel, *Test-area simulation method for the direct determination of the interfacial tension of systems with continuous or discontinuous potentials*, J. Chem. Phys. 123 (2005), 134703.

[24] J.G. Kirkwood and F.P. Buff, *The statistical mechanical theory of surface tension*, J. Chem. Phys. 17 (1949), pp. 338–343.

[25] J.H. Irving and J.G. Kirkwood, *The statistical mechanical theory of transport processes. IV. The equations of hydrodynamics*, J. Chem. Phys. 18 (1950), pp. 817–829.